EXPERIMENTAL INVESTIGATION OF DYNAMIC TORQUE CHARACTERISTICS OF A ROTATING DRAG BODY IN GRANULAR MEDIA

Chundong Liu[1,2], Xiaopu Hao[1], Qiang Zhang[1,2,3], Longchuan Li[4], Zhongxu Sang[1] and Shuai Kang[5][0000-0002-4346-0889]
[1]School of Mechanical Engineering, Hebei University of Architecture, Zhangjiakou 075000, China
[2]Hebei Technology Innovation Center for Intelligent Production Line of Prefabricated Building Components,Hebei University of Architecture, Zhangjiakou 075000, China
[3]Department of Robotics, Ritsumeikan University, Kusatsu, 525-8577, Shiga, Japan
[4]College of Information Science and Technology, Beijing University of Chemical Technology- Beijing 100029, China
[5]College of Mechanical and Electrical Engineering, Beijing University of Chemical Technology- Beijing 100029, China
Email: zq2284@hebiace.edu.cn, kangshuai@buct.edu.cn

Abstract - Rotational interaction between solid bodies and granular media remains insufficiently understood, particularly with respect to the dynamic torque response that plays a critical role in many engineering and robotic applications. To address this gap, this study develops a modular mechatronic drag-testing platform integrating a six-axis force sensing system for high-precision measurement of torque and residual loads under controlled rotational motion. By systematically varying the oscillation amplitude (10°, 30°, 50°, 70°, 90°), input frequency (0.5, 1.0, 1.5 Hz), the waiting interval between the end of one oscillation and the start of the next (0 and 12 s), and drag-body length (250, 300, 350, 400, 450 mm), the dynamic torque response of the granular medium is quantitatively characterized. Experimental results show that peak torque increases significantly with oscillation amplitude and frequency, whereas the residual torque is largely independent of these parameters but grows approximately linearly with drag-body length, and neither peak nor residual torque is affected by the waiting interval.

Keywords: Granular media; Rotational interaction; Dynamic torque response; Residual torque; Mechatronic measurement platform.

1. Introduction

Granular media are widely encountered in natural environments and engineering applications, including planetary surfaces, geological deposits, bulk material handling, and robotic locomotion in unstructured terrains. Unlike classical solids or fluids, granular media exhibit complex mechanical behavior governed by particle–particle contacts, friction, and force-chain networks, leading to highly nonlinear and history-dependent responses[1-3]. Understanding the interaction between solid bodies and granular media is therefore essential for the design and operation of engineering systems such as planetary exploration mechanisms, drilling devices, and bio-inspired robots operating in sandy or particulate environments[4-10].

Early studies on granular media primarily focused on quasi-static translational drag experiments. Aghda[11] elucidated the geometric driving effect of asymmetric flow fields on translational resistance during axial versus lateral intrusion through systematic experiments; Artoni[12] successfully revealed the modulation mechanism of wet environments on the macro-shear resistance of granular media by introducing liquid bridge forces; some scholars focused on dynamic impact conditions, jointly clarifying the grazing ricochet patterns and surface topological deformation characteristics during low-velocity intrusion[13-16]; whereas multiple scholars combined discrete element simulations with advanced optical visualization techniques to thoroughly deconstruct the dynamic rearrangement, strain evolution, and macro-resistance mapping mechanisms of internal

dx.doi.org/10.17683/ijomam/issue24.32

force chain networks within granular materials from a microscopic perspective [17-25].

In contrast to translational motion, rotational actuation induces complex rearrangement of surrounding particles and asymmetric force transmission, resulting in time-varying torque responses[26]. For mechatronic systems, torque is a critical quantity that directly determines actuator selection, structural strength, and control strategy. Despite its importance, the dependence of rotational drag torque on motion parameters and geometric characteristics remains insufficiently quantified, largely due to the lack of dedicated experimental platforms capable of high-precision torque measurement under controlled rotational conditions.

Only a limited number of studies have begun to address rotational intrusion scenarios. For example, Guillard et al. [27] investigated the resistance experienced by a rotating cylindrical rod in granular media, highlighting the difference in drag force between the first rotation cycle and subsequent cycles and attributing this behavior to rotation-induced particle rearrangement. However, these studies primarily focused on force variations and did not perform systematic measurements or quantitative analyses of the torque generated during rotational motion. Consequently, the torque response of granular media under rotational actuation, as well as its dependence on geometric and motion parameters, remains insufficiently characterized at the experimental level.

Existing experimental studies often rely on simplified setups or indirect measurements, focusing primarily on force components rather than torque, or treating rotational effects as secondary phenomena. Moreover, systematic investigations that simultaneously consider oscillation amplitude, input frequency, geometric dimensions, and temporal loading conditions are still scarce. These limitations hinder the development of reliable mechanical models and design guidelines for rotationally actuated systems interacting with granular media.

To address these challenges, this study develops a modular mechatronic rotational drag-testing platform equipped with a six-axis force sensing system, enabling high-precision measurement of torque under controlled rotational motion. The platform allows systematic variation of oscillation amplitude, input frequency, drag-body length, and the waiting interval between successive oscillation cycles, providing a controlled experimental framework for quantitative analysis of rotational drag behavior in granular media.

Using this platform, a series of rotational drag experiments are conducted to investigate the dynamic torque response of granular media. The effects of oscillation amplitude, actuation frequency, drag-body length, and waiting interval on both peak and residual torque are examined in detail. The results reveal distinct roles of motion parameters and geometric factors in governing torque characteristics, offering new experimental insights into rotational interactions between solid bodies and granular media.

The remainder of this paper is organized as follows. Section 2 describes the design and configuration of the rotational drag mechatronic platform, including the actuation system and force sensing setup. Section 3 presents the experimental procedures and discusses the effects of key parameters on rotational drag torque. Finally, Section 4 summarizes the main findings and outlines their implications for engineering design and future research.

2. Rotational Drag Mechatronic Platform

2.1 Drag Body and Granular Material Properties

Observations indicate that animals inhabiting loose granular media, such as sand snakes, commonly exhibit a distinctive body morphology characterized by an arched dorsal surface and a flattened ventral surface, as shown in Figure 1(a). This morphology is not incidental: the arched back effectively redistributes the pressure exerted by the overlying particles, thereby reducing sinking resistance, while the flattened belly provides a stable support interface that helps maintain balance during locomotion.

Zhu et al. [28] introduced a simplified snake-like model that utilizes the rotational velocity field at maximum curvature points for propulsion. This mechanism allows for sinusoidal-driven progression independent of anisotropic friction. Owing to its physical alignment with the movement of snakes and sandfish in water or sand, this isotropic and structurally uniform model is employed to bypass biological complexities. Analyzing its kinematics and energy efficiency reveals the core physical principles governing similar natural undulatory locomotion.

In the study by Chen et al., the model is idealized as a slender beam resting on a rigid horizontal substrate. The geometric characteristics of the beam are defined by its length L, width b, and height h, while its mechanical attributes are determined by the Young's modulus E, Poisson's ratio v, and mass density ρ. The z-axis of the system is oriented in the direction opposite to the gravity vector. To ensure a simplified physical environment, the model assumes that all material and surface properties, including the friction coefficient, are spatially isotropic and uniformly distributed. To characterize its kinematic features, a local curvilinear coordinate system (s, n) is introduced, which follows the movement of the beam's centerline. Within this framework, s represents the arc length measurement, n denotes

the normal displacement, and θ characterizes the evolution of the tangent angle. Figure 1(b) illustrates the schematic diagram of the soft beam model actuated by a snake-like traveling sinusoidal wave propagating from left to right.

The deformation of the system is driven by a periodic sinusoidal traveling wave propagating along the axis, with its curvature function expressed as Formula (1).

$$k(s,t) = k_0 \sin[2\pi(t - s)] \quad (1)$$

Where, k_0 corresponds to the maximum curvature at the wave crest. Both time t and arc length s are non-dimensionalized, being normalized against the lateral motion period P and the wavelength λ, respectively.

Inspired by this natural adaptation, the present study adopts a similar biomimetic geometry for the drag body moving through granular media. The geometry and dimensions of the drag body are illustrated in Figures 1(c) and 1(d), and the corresponding parameters are summarized in Table 1. This design ensures sufficient traction while suppressing excessive sinking. Moreover, the biomimetic form favorably regulates the granular flow around the body, enabling a balance between reduced motion resistance and enhanced stability.

(a) Sand snake

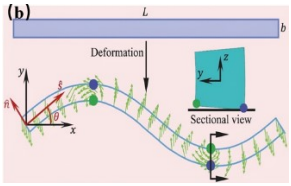

(b) Schematic of a snake-like soft beam model

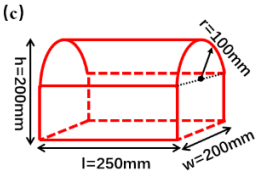

(c) Size diagram of the drag body

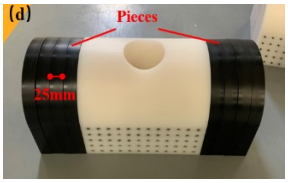

(d) Physical pictures of the drag body and additional pieces

Figure 1: The biological shapes in nature and the shapes of drag body

Table 1. Parameters of the rotational drag body

Dimension	250 mm×200 mm×200 mm
Mass	10.8 kg
Moment of Inertia	6.61×10^{-2} kg·m^2
Material	Polyoxymethylene

2.2 Platform Design

The experimental platform is illustrated in Figure 2. The rotary motion module is integrated through an aluminum-profile flange structure, onto which the servo motor, speed reducer, six-axis force sensor, steel pipe connector, and drag body are sequentially mounted. The key parameters of each component of the experimental platform are summarized in Table 2.

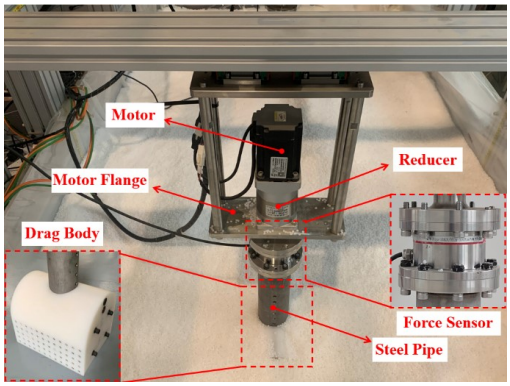

Figure 2: Schematic diagram of rotating drag platform

Table 2. The mass and rotational inertia of each component of the platform

Component	Mass (kg)	Rotational inertia (kg·m^2)
Motor	3.8	2.97×10^{-4}
Reducer	5	5.06×10^{-3}
Force sensor	4.2	4.88×10^{-3}
Steel pipe	7.6	1.28×10^{-1}
Drag Body	10.8	6.61×10^{-2}

The bottom of the platform is filled with granular material, within which the drag body is fully embedded during the experiments. The relevant physical parameters of the granular medium are listed in Table 3.

Table 3. Parameters of granular media

Ingredient	polyethylene
Density	ρ = 0.92 g/cm^3
Dimension	average diameter is 6mm
Shape	irregular ellipsoids

The six-dimensional force sensor (DECENT γ125) is used to measure the forces and torques along the x-, y-, and z-directions. It has a maximum load capacity of 500 N·m and a minimum force resolution of 0.5 N·m.

The detailed parameters of the combined motor are shown in Table 4.

Table 4. Parameters of the combined motor (including the reducer)

Model	LCMT - 10L - 80M04D25
Rated power	1 kW
Rated torque	100 N·m
Rated rotational speed	100 rpm

The calculation formula for the rotational speed of the combined motor is shown in Formula (2).

$$n = \frac{120\theta f}{\pi}(\text{rpm}) \quad (2)$$

3. Rotational Drag Experiments

3.1 Experimental Parameter Design and Procedure

The drag body undergoes a prescribed rotational sequence of counterclockwise → clockwise → clockwise → counterclockwise → counterclockwise → clockwise, completing a total of 1.5 cycles. This sequence incorporates both a single alternation between forward and reverse rotation and two successive rotations in the same direction. A schematic illustration of the rotation protocol is provided in Figure 3. To minimize the influence of measurement uncertainty, each experimental condition was repeated three times. The experimental variables include the rotation amplitude (10°, 30°, 50°, 70°, and 90°), input frequency (0.5, 1.0, and 1.5 Hz), waiting time between successive rotations (0 and 12 s), and the length of the drag body (250, 300, 350, 400, and 450 mm).

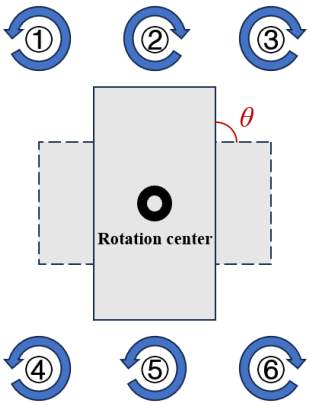

Figure 3: Schematic diagram of the rotation sequence of the drag body in the experiment

At the beginning of each experiment, the granular material was excavated until the drag body was fully exposed, as shown in Figure 4. This procedure was conducted to eliminate any residual torque within the granular medium. The particles were then backfilled until the drag body was just completely buried, after which all force sensor readings were reset to zero. Subsequently, real-time torque data were recorded during the rotation of the drag body.

Figure 4: The drag body at the beginning of the experiment

3.2 Experimental Data Analysis

Based on the experimental setup and procedures described above, a series of systematic experiments was performed to investigate the torque response of granular media under rotational dragging. The influences of experimental repeatability, waiting time, swing amplitude, swing frequency, and drag-body geometry on peak and residual torque were analyzed in detail. Supplementary videos illustrating representative experimental processes are provided in the accompanying materials.

3.2.1 Verification of Experimental Repeatability

Following the experimental procedure described above, three repeated trials were conducted under conditions of a swing amplitude of 90°, an input frequency of 1.5 Hz, and zero waiting time between the six successive rotations. The corresponding experimental results are presented in Figure 5.

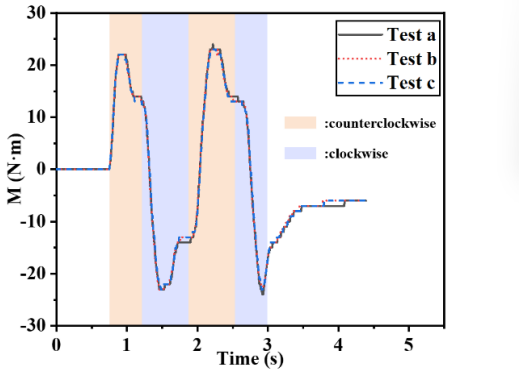

Figure 5: The results of three repeated experiments under the conditions of a 90° swing amplitude, an input frequency of 1.5 Hz, and no waiting time between six rotational movements

The experimental data exhibit excellent repeatability and consistency. Across the three trials, the peak torque values were consistently

approximately 23 N·m, while the residual torque after rotation stabilized at around 6 N·m in each case. The torque–time curves from the three measurements show a high degree of agreement in terms of overall trend, fluctuation amplitude, and phase characteristics. These results indicate that the granular medium state, motion control, and data acquisition system maintained a high level of stability and reliability throughout the experiments.

During the rotational dragging experiments in the granular medium, pronounced dynamic effects were observed. In the tests with a swing amplitude of 90°, the motor transmission system reached its torque limit while opposing the periodically reversing high-load motion, causing the actual motor operating frequency to be lower than the commanded input frequency. Specifically, when the input frequency was set to 1.5 Hz, the measured output rotational frequency was approximately 0.65 Hz; for an input frequency of 1.0 Hz, the actual output frequency decreased to about 0.62 Hz; and for an input frequency of 0.5 Hz, the corresponding output frequency was approximately 0.45 Hz.

3.2.2 Effect of Waiting Time on the Torque Acting on the Drag Body

To investigate the influence of waiting time on the experimental outcomes, a comparative study was conducted between a continuous rotation mode (without waiting) and an intermittent rotation mode, in which a 12 s pause was introduced after each rotation. In both cases, the input frequency was set to 1.5 Hz and the swing amplitude to 90°. The corresponding experimental results are presented in Figure 6. Experimental videos regarding the presence or absence of a waiting interval are provided in Video 5 and Video 8 in the accompanying materials.

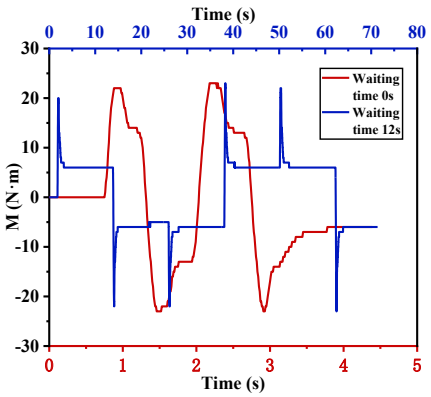

Figure 6: The torque-time response curves of the towed object under two typical operating conditions: continuous rotation mode (without waiting) and intermittent rotation mode (waiting for 12 seconds after each rotation), with an input frequency of 1.5 Hz and a swing amplitude of 90°

From an overall perspective, the peak magnitudes of the two curves are nearly identical, indicating that the peak torque exhibits no significant dependence on the waiting duration following each rotation. This observation implies that the maximum resistive torque arising from the forced reorganization of the granular medium as the drag body initiates rotation and reaches its maximum angular displacement is predominantly governed by the geometric conditions of the motion, and is largely independent of the medium's relaxation process after the preceding rotation.

Under the 12 s waiting condition, the torque does not immediately decay to zero after each rotation; instead, it stabilizes at approximately ±6 N·m and remains nearly constant throughout the waiting interval. This behavior clearly indicates the presence of residual stress retained within the granular medium following each rotation. Moreover, the stability of this residual torque suggests that it represents an inherent and persistent mechanical response of the granular system under the specified rotational conditions.

3.2.3 Effect of Swing Amplitude on the Peak Torque Acting on the Drag Body

To evaluate the effect of rotational amplitude on the peak torque, a series of rotational experiments were performed with varying amplitudes. In all tests, the input rotational frequency was fixed at 1.5 Hz and a waiting time of 12 s was imposed between successive rotations. The corresponding experimental results are presented in Figure 7. Experimental videos corresponding to different oscillation amplitudes are provided in Video 1 to Video 5 in the accompanying materials.

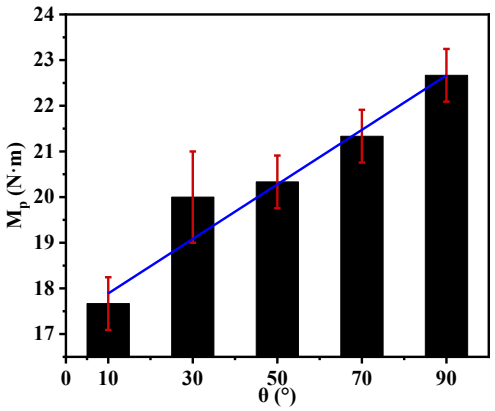

Figure 7: The variation relationship of the peak torque corresponding to different rotational swing amplitudes under the conditions of an input rotational frequency of 1.5 Hz and a waiting time of 12 seconds

The peak torque increases monotonically with rotational amplitude, indicating that larger rotational disturbances induce stronger shear within the granular medium, thereby generating greater resistance. The expression derived from the known data using the least squares method is presented in Formula (3). Where M_p represents the peak torque acting on the rotating drag body in N·m , and θ denotes the oscillation amplitude of the rotating drag body in degrees (°). The values of θ are taken as 10°、30°、50°、70° and 90°. The root-mean-square error (RMSE) of the fit is 0.46.

$$M_p = 0.06\theta + 17.29 \quad (3)$$

The error bars represent the standard deviation obtained from three repeated trials; their small magnitude reflects good experimental repeatability and system stability. If there is no error bar in the figure, it indicates that the regression of the three groups of experimental values is consistent, and the standard deviation is 0. These results demonstrate that rotational amplitude is a key control parameter governing torque magnitude. Increasing the amplitude enlarges the disturbed zone, enhances energy dissipation, and promotes more frequent breakage and reformation of force chains. This finding provides an experimental basis for the quantitative prediction of torque and for the energy-efficient regulation of rotational resistance in granular media.

3.2.4 Effect of Swing Frequency on the Peak Torque Acting on the Drag Body

To investigate the influence of input rotational frequency on the peak torque, a series of rotational experiments were carried out at different input frequencies. In all cases, the waiting time between successive rotations was fixed at 12 s. The corresponding experimental results are presented in Figure 8. Experimental videos corresponding to different frequencies are provided in Video 5 to Video 7 in the accompanying materials.

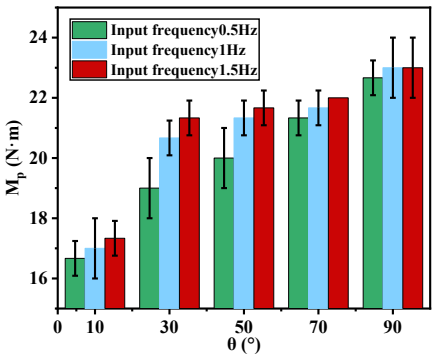

Figure 8: The influence of different rotational frequencies on the peak torque at each swing amplitude under a waiting time of 12 seconds

For a given rotational amplitude, the peak torque increases systematically with input frequency, demonstrating a pronounced rate dependence. However, due to hardware limitations, the actual rotational frequency of the drag body could not reach the configured input frequency. Consequently, we could only establish qualitative trends rather than deriving precise mathematical formulas. At higher frequencies, the time available for contact force transmission and grain rearrangement is reduced, preventing the granular assembly from fully accommodating the externally imposed loading. Consequently, stronger inertial resistance and dynamic strengthening effects emerge. Moreover, increasing the rotation frequency intensifies dilatancy, leading to modifications in the local packing fraction and a further increase in shear resistance.

3.2.5 Effect of Swing Amplitude on the Residual Torque Acting on the Drag Body

To assess the effect of rotational amplitude on the residual torque after rotation, a series of rotational experiments were performed with varying amplitudes. In all tests, the input rotational frequency was fixed at 1.5 Hz and the waiting time was set to 12 s. The corresponding experimental results are presented in Figure 9.

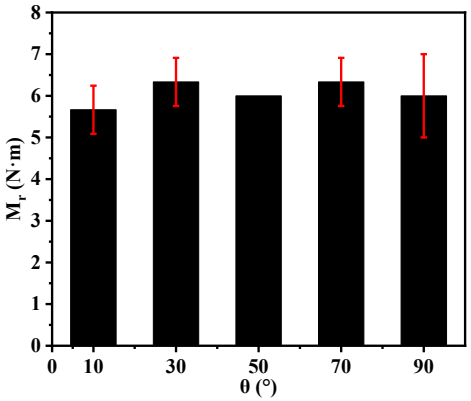

Figure 9: The relationship between rotational amplitude and residual torque under conditions of an input rotational frequency of 1.5 Hz and a waiting time of 12 seconds

The residual torque remains relatively low and confined within a narrow range (approximately 5.5–6.5 N·m) for rotational amplitudes spanning from 10° to 90°. Particularly when the oscillation amplitude of the drag body is 50°, the results from the three experimental trials are nearly identical, leading to very small error bars. From a mechanistic standpoint, this observation indicates that stress relaxation within the granular medium is largely completed within the 12 s waiting period. Regardless of the initial rotational amplitude, the system is able to substantially dissipate the internal stresses

generated during rotation through microstructural rearrangement, allowing the force-chain network to return to a quasi-equilibrium state. The slight variations observed are more likely attributable to measurement uncertainty or the inherent stochasticity of granular reconfiguration, rather than to systematic amplitude-dependent effects.

3.2.6 Effect of Swing Frequency on the Residual Torque Acting on the Drag Body

To investigate the effect of input rotational frequency on the residual torque after rotation, a series of rotational experiments were performed at different input frequencies. In all cases, the waiting time between successive rotations was fixed at 12 s. The corresponding experimental results are presented in Figure 10.

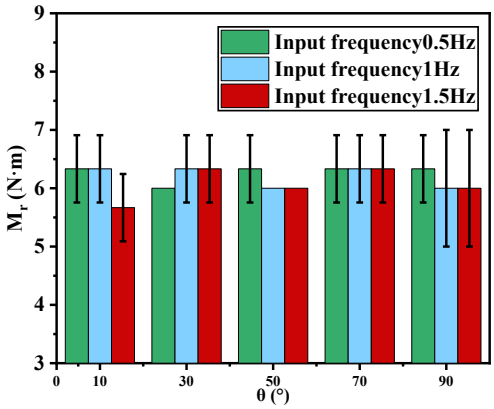

Figure 10: The influence of different rotational frequencies on the residual torque at each swing amplitude, with a waiting time of 12 seconds

The residual *torque* maintains a narrow range (approximately 5.5–6.5 N·m) across all tested frequencies, exhibiting no discernible frequency dependence. This finding indicates that when adequate recovery time is allotted, the ultimate residual *torque* state becomes impervious to the preceding motion rate. Following the cessation of rotation, the medium undergoes a process of full stress relaxation through micro-sliding and force-chain reconfiguration. This dissipates the elastic strain energy that has been introduced by rotations at different frequencies, thus returning the medium to a common stress equilibrium state.

3.2.7 Effect of Drag Body Length on the Torque Acting on the Drag Body

To examine the influence of the drag body length on both the peak torque and the residual torque after rotation, a series of rotational experiments were performed with varying drag body lengths. The experimental conditions were fixed at an oscillation amplitude of 90°, an input rotational frequency of 1.5 Hz, and a waiting time of 12 s. The corresponding experimental results are presented in Figure 11. Experimental videos regarding the increase in the length of the drag body are provided in Video 9 in the accompanying materials.

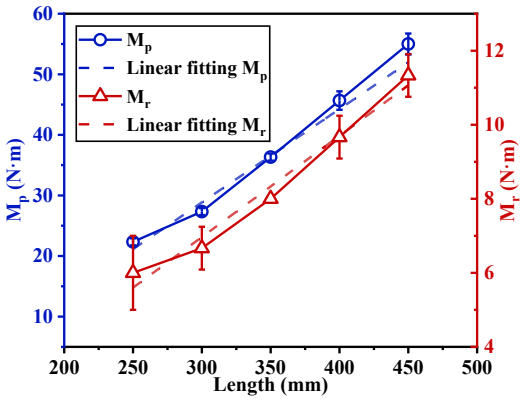

Figure 11: The influence of the drag body length on peak torque and residual torque at the end of the rotation cycle, under conditions of a 90° rotation, an input frequency of 1.5 Hz, and a waiting time of 12 seconds

The peak torque increases approximately linearly with the length of the drag body. The expression derived from the known data using the least squares method is presented in Formula (4). Where M_p represents the peak torque acting on the rotating drag body in N·m, and L denotes the length of the rotating drag body in mm. The values of L are taken as 250 mm, 300 mm, 350 mm, 400 mm, and 450 mm. The root-mean-square error (RMSE) of the fit is 1.74.

$$M_p = 0.15L - 17.39 \tag{4}$$

This behavior can be attributed to the increase in effective contact area, which entails a larger number of grains participating in the formation and rupture of force chains. In addition, the change in overall geometry induces more complex granular flow patterns and enhances anisotropic stress distributions during rotation, thereby further increasing the resistive torque.

The variation in residual torque indicates that it also increases with the length of the drag body in an approximately linear relationship. The expression derived from the known data using the least squares method is presented in Formula (5). Where M_r represents the residual torque after the rotation of the drag body in N·m, and L denotes the length of the rotating drag body in mm. The root-mean-square error (RMSE) of the fit is 0.29.

$$M_r = 0.03L - 1.23 \tag{5}$$

Two primary mechanisms are responsible: (i) a larger contact area mobilizes more grains within the force-chain network, thereby enhancing the medium's capacity for stress storage; and (ii) an

expanded disturbance region promotes more profound microstructural rearrangements, leading to increased accumulation of elastic strain energy within the granular assembly.

4. Conclusions

Through systematic experimentation and comprehensive data analysis, this study elucidates the effects of rotational amplitude, input frequency, waiting interval, and drag body size on the torque response of a granular medium. First, the results characterize the torque response under rotational motion, showing that the peak torque increases markedly with rotational amplitude, thereby confirming that large-angle rotations expand the extent of particle rearrangement and intensify energy dissipation. Second, a clear rate-dependent behavior is identified, with the peak torque exhibiting a monotonic increase as the input frequency rises. Third, the experiments verify the stress self-recovery capability of the granular medium: a waiting time of 12 s is sufficient for the system to largely restore its stress state after rotation. Finally, the study systematically demonstrates the pronounced influence of geometric scale, revealing that both the peak torque and the residual stress increase significantly with drag body size, with the peak torque displaying an approximately linear dependence on length. Through experiments characterized by high reliability and repeatability, the following specific conclusions were obtained:

1) Under specific rotational frequencies and oscillation amplitudes, the peak torque generated during the rotation of the drag body is independent of the waiting interval.

2) Under conditions of a specific rotational frequency and a set waiting interval, the peak torque increases almost linearly with oscillation amplitude.

3) Under the condition of having a waiting interval, the peak torque increases with the increase of frequency.

4) Under conditions of a specific rotational frequency and a set waiting interval, the residual torque remaining after the rotation of the drag body is independent of both the oscillation amplitude and input frequency.

5) Under conditions of a specific rotational frequency, oscillation amplitude, and a set waiting interval, both the peak torque generated during the rotation of the drag body and the residual torque after rotation show an almost linear relationship with the length of the drag body.

In terms of engineering applications, the results of this study provide important references for the optimization of planetary probe wheel design, the selection of drilling equipment parameters, etc. At the same time, the research results can be extended to fields such as bionic robots and geological disaster prevention, exploring broader application scenarios. The advancement of these research directions will contribute to the establishment of a more complete particle medium mechanics theoretical system and provide continuous theoretical support for the development of related engineering technologies.

Acknowledgements

This work is supported in part by the Science and Technology Research Project of Colleges and Universities in Hebei Province under Grant ZC2023140, and in part by the Talent Engineering Project in Hebei Province under Grant C20231128,and the National Natural Science Foundation of China (No. Grant 42506180, 62273340), by the Fundamental Research Funds for the Central Universities, China (Grant No. buctrc202215), by the LiaoNing Revitalization Talents Program, China (Grant No. XLYC2403108), and by the Key Research and Development Projects of Liaoning Province, China (Grant No. 2024JH2/102400045).

References

[1] K. Farain, D. Bonn, Quantitative Understanding of the Onset of Dense Granular Flows, Physical Review Letters 130(10) (2023) 108201. DOI: https://doi.org/10.1103/PhysRevLett.130.108201

[2] W. Liu-Fu, H. Xiao, J. Chen, et al., Unique Viscoelasticity and Hierarchical Relaxation Dynamics of Molecular Granular Materials, Nano Letters 24(11) (2024) 3307-3314. DOI: https://doi.org/10.1021/acs.nanolett.4c00045

[3] N. Deng, A. Wautier, A. Tordesillas, et al., Lifespan dynamics of cluster conformations in stationary regimes in granular materials, Physical Review E 105(1) (2022) 014902. DOI: https://doi.org/10.1103/PhysRevE.105.014902

[4] A.J.R. Lopez-Arreguin, S. Montenegro, Towards bio-inspired robots for underground and surface exploration in planetary environments: An overview and novel developments inspired in sand-swimmers, Heliyon 6(6) (2020) e04148. DOI: https://doi.org/10.1016/j.heliyon.2020.e04148

[5] J. Liu, Y. Tong, J. Liu, Review of snake robots in constrained environments, Robotics and Autonomous Systems 141 (2021) 103785. DOI: https://doi.org/10.1016/j.robot.2021.103785

[6] Y. Cao, L. Li, Z. Ma, et al., Investigation of efficient creeping locomotion for snake-like robots with compliant passive joints, Biomimetic Intelligence and Robotics 6(1) (2026) 100281. DOI: https://doi.org/10.1016/j.birob.2026.100281

[7] S.K.R. Moosavi, M.H. Zafar, F. Sanfilippo, Snake robots: A state-of-the-art review on design, locomotion, control, and real-world applications, Mechatronics 112 (2025) 103418. DOI:

https://doi.org/10.1016/j.mechatronics.2025.103418

[8] B.A. Trimmer, Metal or muscle? The future of biologically inspired robots, Science Robotics 5(38) (2020) eaba6149. DOI: https://doi.org/10.1126/scirobotics.aba6149

[9] X. Liu, S. Wen, Y. Hu, et al., An active SLAM with multi-sensor fusion for snake robots based on deep reinforcement learning, Mechatronics 103 (2024) 103248. DOI: https://doi.org/10.1016/j.mechatronics.2024.103248

[10] Y. Tang, J. Tao, Multiscale analysis of rotational penetration in shallow dry sand and implications for self-burrowing robot design, Acta Geotechnica 17(10) (2022) 4233-4252. DOI: https://doi.org/10.1007/s11440-022-01538-4

[11] S.A. Aghda, A. Naji, Drag force on cylindrical intruders in granular media: Experimental study of lateral vs axial intrusion and high grain-size polydispersity, Powder Technology 415 (2023) 118194. DOI: https://doi.org/10.1016/j.powtec.2022.118194

[12] R. Artoni, G. Loro, P. Richard, et al., Drag in wet granular materials, Powder Technology 356 (2019) 231-239. DOI: https://doi.org/10.1016/j.powtec.2019.08.023

[13] J. Liu, Z. Wang, Y. Tian, et al., Drag force modeling with induced surface deformation in granular media, Powder Technology 455 (2025) 120757. DOI: https://doi.org/10.1016/j.powtec.2025.120757

[14] E. Wright, A.C. Quillen, J. South, et al., Ricochets on Asteroids: Experimental study of low velocity grazing impacts into granular media, Icarus 351 (2020) 113963. DOI: https://doi.org/10.1016/j.icarus.2020.113963

[15] A.V. Yennemadi, D.V. Khakhar, Drag, lift, and buoyancy forces on a single large particle in dense granular flows, Physical Review Fluids 8(7) (2023) 074302. DOI: https://doi.org/10.1103/PhysRevFluids.8.074302

[16] F. Patino-Ramirez, C.O. Sullivan, Optimal tip shape for minimum drag and lift during horizontal penetration in granular media, Acta Geotechnica 19(1) (2023) 19-38. DOI: https://doi.org/10.1007/s11440-023-01896-1

[17] X. Zhang, H. Zhao, Y. Wang, et al., The effect of particle shape on the dynamics of spherical projectile impacting into granular media, Computational Particle Mechanics 11(6) (2024) 2677-2692. DOI: https://doi.org/10.1007/s40571-023-00693-w

[18] L. Li, Z. Song, Q. Zhang, X. Hao, C. Liu, S. He, S. Chen, S. Kang, Experimental investigation for wedge interaction with granular media, Europhysics Letters 151(6) (2025) 63001. DOI 10.1209/0295-5075/ae049a

[19] K. Ju, T. Zhao, Y. Luo, et al., Force chain generation and evaluation of granular materials based on discrete element simulation and generative adversarial network, Powder Technology 461 (2025) 121100. DOI: https://doi.org/10.1016/j.powtec.2024.121100

[20] M. Wu, F. Yang, H. Jiang, et al., Visualization of particle micro-rotations and strain (force) chain in granular materials using three-dimensional electronic speckle pattern interferometry, Optics & Laser Technology 186 (2025) 112642. DOI: https://doi.org/10.1016/j.optlastec.2024.112642

[21] B. Świtała, D. Leśniewska, M.A. Kalwar, Micro-mechanisms of force network rearrangement in granular materials, Computers and Geotechnics 174 (2024) 106602. DOI: https://doi.org/10.1016/j.compgeo.2024.106602

[22] A.A. Zaidi, Granular drag force during immersion in dry quicksand, Powder Technology 364 (2020) 986-993. DOI: https://doi.org/10.1016/j.powtec.2020.01.070

[23] F. Chen, Y. Liu, Y. Wang, et al., Deformation and Force Chain of Two-Dimensional Granular Systems under Continuous Loading, Materials 16(15) (2023) 5441. DOI: https://doi.org/10.3390/ma16155441

[24] R. Mandal, C. Casert, P. Sollich, Robust prediction of force chains in jammed solids using graph neural networks, Nature Communications 13(1) (2022) 31732. DOI: https://doi.org/10.1038/s41467-022-31732-3

[25] Y. Wang, J. Shang, Y. Wang, J. Zhang, Contact force measurements and local anisotropy in ellipses and disks, Physical Review Research 3(4) (2021) 043053. DOI: https://doi.org/10.1103/PhysRevResearch.3.043053

[26] S. Agarwal, A. Karsai, D.I. Goldman, et al., Surprising simplicity in the modeling of dynamic granular intrusion, Science Advances 7(17) (2021) eabe0635. DOI: https://doi.org/10.1126/sciadv.abe0635

[27] Guillard F, Forterre Y, Pouliquen O. Lift forces in granular media[J]. Physics of Fluids, 2014, 26(4): 043301. DOI:10.1063/1.4869859

[28] Zhu, L., Yang, P., Li, F., Wang, K., Shui, L., Chen, X., On the snake-like lateral un-dulatory locomotion in terrestrial, aquatic and sand environments, Journal of the Mechanics and Physics of Solids 157 (2021) 104629. DOI: https://doi.org/10.1016/j.jmps.2021.104629